Journal of Circuits, Systems, and Computers
Vol. 20, No. 7 (2011) 1287–1301

DOI: 10.1142/S021812661100789X

World Scientific
www.worldscientific.com

MODELING OF EDDY CURRENT LOSS AND TEMPERATURE OF THE MAGNETS IN PERMANENT MAGNET MACHINES*

XIAOFENG DING

Electrical Engineering Department,
Northwestern Polytechnical University,
127 Youyi Xilu #352, Xi'an, Shaanxi 710072, China
dxf_219@163.com

CHRIS MI

Electrical and Computer Engineering Department,
University of Michigan-Dearborn, 4901 Evergreen Road,
Dearborn, Michigan 48128, USA
chrismi@umich.edu

Received 24 November 2010
Accepted 16 June 2011

The eddy current loss in the magnets of permanent magnet (PM) motors in a hybrid electric vehicle (HEV) and plug-in HEV is usually not taken into consideration in traditional motor design and analysis. However, due to the high conductivity of the rare-earth magnet, neodymium-iron-boron (NdFeB), and slot/tooth harmonics, there is eddy current loss generated inside the magnets. This loss may not attribute very much to the efficiency of the motor, but the temperature-rise inside the magnets caused by this loss can lead to the unpredictable deterioration of the magnets, such as the degradation of performance and potential demagnetization. In addition, the output voltage of pulse-width-modulated (PWM) inverter contains abundant high frequency harmonics, which induce excessive loss in the magnets. The excessive heat in PM motor induced by the eddy current loss combined with other losses can degrade the performance of the machine. This paper presents the modeling and analysis of eddy current loss in surface-mounted-magnets PM synchronous motors (SPMSM) and interior-magnets PM synchronous motors (IPMSM), operated by PWM inverter supply. Analytical methods are implemented, in conjunction with time-stepped finite-element analysis (FEA) for the calculation of eddy current loss in the magnet. Based on the calculated losses in the machines, simplified analytical models are developed as thermal circuits with network of interconnected nodes, thermal resistances and heat sources representing the heat processes within the SPMSM and IPMSM, to predict the temperature of the magnets. The predicted machine temperatures are found to be consistent with the experimental measurement.

Keywords: Pulse-width-modulated (PWM); surface-mounted-magnets PM synchronous motors (SPMSM); interior magnet PM motors; time-stepped finite-element analysis (FEA); thermal circuits; demagnetization; hybrid electric vehicles; electric vehicles; vehicle powertrain.

*This paper was recommended by the Regional Editor Krishna Shenai.

1. Introduction

Due to tighter fuel economy constraints, awareness of environment issues and the shortage of oil supply, electric vehicles (EV), hybrid electric vehicles (HEV) and plug-in hybrid electric vehicles (PHEV) have attracted a lot attention lately. Permanent magnet (PM) motors are popular choices for EV/HEV/PHEV traction drives, either PM synchronous motors (PMSM) or PM brushless DC motors (BLDC), due to their many advantages, such as the higher efficiency, smaller size, and larger torque capability. The rare-earth magnets, neodymium-iron-boron (NdFeB), are used in these motors due to its high energy density. However, the relatively high conductivity of the magnet manifests an eddy current loss inside the magnets.[1,2] Although this loss may not attribute very much to the efficiency of the motor, it will result in a temperature-rise inside the magnets. In addition, the output voltage of pulse-width-modulated (PWM) inverter that is used to drive the PM motors contains abundant high frequency harmonics, which induce excessive losses in the motor.[3] Hence, excessive temperature-rise can exist in PM motors. Such temperature-rise will degrade the performance of the PM motors and may cause irreversible demagnetization of the magnets.[4–7]

Until recently, there has been a large emphasis on the electromagnetic properties of such a motor. However, the potential demagnetization due to excessive temperature-rise of the magnets can negatively impact the large deployment of EV/HEV/PHEV. The optimal design of electrical motors with solid thermal characteristics[8–18] will provide improved efficiency and power densities in traction motors. The thermal complexities involved in developing motors require a breakdown of the individual thermal components in the system.

This paper depicts the eddy current loss density in a two-dimensional (2D) polar coordinate referring to Refs. 19–23 for surface-mounted PM synchronous motors (SPMSM) and presents a reliable analytical method for the eddy current loss calculation of interior-magnet PM synchronous motors (IPMSM). These models are also applicable to brushless PM motors. Subsequently, the output voltage of PWM supply is divided into fundamental voltage and high frequency harmonic voltages. The latter gives the incremental losses in the machine. The results from the analytical models are compared with the results from the corresponding time-stepped finite-element analysis (FEA) and measurement to validate the proposed models.

Starting from the eddy current loss combined with other losses within the machines, simplified thermal models for SPMSM and IPMSM are developed respectively in this paper. These are represented through thermal circuits that incorporate conduction and convection behavior and the thermal resistances and sources of the motors. Radiation is neglected due to the minor effect it has on such systems. The thermal circuits are then solved through a system of linear equations. The described temperature profiles within the machines are compared with experimental measurement on the Toyota Prius HEV traction motor.

2. Eddy Current Loss in the Magnets of SPMSM

The stator winding is modeled as an equivalent current sheet.[23] In order to obtain an expression for the current sheet of the winding, the current sheet of one coil in two slots is considered. Figure 1 shows the current sheet that is distributed along the slot openings b_0 uniformly.

The winding pitch of the motor is 5 times the length of the slot pitch in this paper. Therefore the expression of the current sheet distribution is obtained as follows:

$$J_a = \begin{cases} \dfrac{i}{b_0}, & -\dfrac{5\alpha_y}{2} - \dfrac{b_0}{2R_S} \le \alpha \le -\dfrac{5\alpha_y}{2} + \dfrac{b_0}{2R_S}, \\ -\dfrac{i}{b_0}, & \dfrac{5\alpha_y}{2} - \dfrac{b_0}{2R_S} \le \alpha \le \dfrac{5\alpha_y}{2} + \dfrac{b_0}{2R_S}, \\ 0, & \text{other}, \end{cases} \tag{1}$$

where α_y is the slot pitch, b_o is the slot opening, R_s is the stator radius and i is the stator current. The Fourier series expansion of (1) is derived as

$$J_a = \sum_v b_v \sin v\alpha = -\frac{2i}{\pi R_S} \sum_v K_{\text{sov}} K_{pv} \sin v\alpha, \tag{2}$$

where

$$K_{\text{sov}} = \frac{\sin v\frac{b_0}{2R_s}}{v\frac{b_0}{2R_s}}, \quad K_{pv} = \sin v\frac{5\alpha_y}{2}$$

and v is the order of space harmonics.

The equivalent current sheet of the 3-phase windings can be obtained after the derivation,

$$J_{abc} = J_{aN} + J_{bN} + J_{cN} = \mp\frac{3N}{\pi R_S} \sum_u I_u \sum_v K_{\text{sov}} K_{pv} K_{dv} \cos(up_r\omega_r t \pm v\alpha + \theta_u), \tag{3}$$

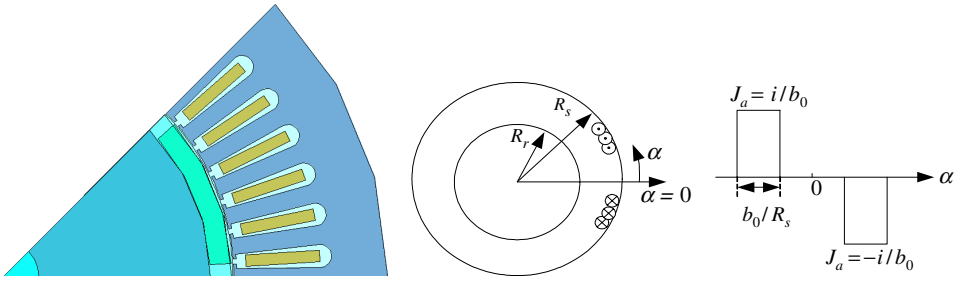

(a) (b) (c)

Fig. 1. Equivalent current sheet model of one coil in slots. (a) Cross sectional area of SPMSM. (b) Stator current assumed to be on the slot opening as a current sheet. (c) Magnitude of stator current distribution.

where N is the number of turns in series per phase, I_u is the amplitude of the harmonic current, ω_r is the rotor angular velocity, p_r is the number of pole-pairs, θ_u is the phase current harmonic angle, and K_{dv} is winding distribution factor.

The magnetic vector potential A can be obtained by the solution of Laplace's equation,[5,19]

$$A(r,\theta_r,t) = \mp\mu_0 \sum_u^\infty \sum_v^\infty \frac{J_{uv} R_s^{-vp_s+1}}{G_v(vp_s)} (r^{vp_s} + R_s^{2vp_s} r^{-vp_s}) \times \cos[(up_r \pm vp_s)\omega_r t \pm vp_s\theta_r + \theta_u], \tag{4}$$

where

$$J_{uv} = \frac{3NI_u}{\pi R_s} K_{\text{sov}} K_{pv} K_{dv}, \quad G_v = 1 - \left(\frac{R_r}{R_s}\right)^{2vp_s}$$

and p_s is the pole-pairs number of the winding MMF, and θ_r is the initial angle of rotor. The induced eddy current in the permanent magnets can be defined as

$$J_m(r,\theta_r,t) = -\sigma \frac{\partial A(r,\theta_r,t)}{\partial t} + C(t), \tag{5}$$

where σ is the electrical conductivity of the magnets, $c(t)$ is an integration constant which makes the net total current flowing in each magnet segment equal to zero at any instant, i.e.,

$$\int_{R_r}^{R_m} \int_{-\frac{\alpha_p}{2}}^{\frac{\alpha_p}{2}} J_m r dr d\theta_r = 0. \tag{6}$$

Therefore, the analytical expression for eddy current density can be derived from (5) and (6),

$$\begin{aligned} J_m(r,\theta_r,t) = {} & \mp\sigma\mu_0 \sum_u^\infty \sum_v^\infty \frac{J_{uv} R_s^{-vp_s+1}}{G_v(vp_s)} (up_r \pm vp_s)\omega_r \\ & \times (r^{vp_s} + R_r^{2vp_s} r^{-vp_s}) \sin[(up_r \pm vp_s)\omega_r t \pm vp_s\theta_r + \theta_u] \\ & \pm \frac{2\sigma\mu_0}{(R_m^2 - R_s^2)\alpha_p} \sum_u^\infty \sum_v^\infty \mp \frac{1}{vp_s} \frac{J_{uv} R_s^{-vp_s+1}}{G_v(vp_s)} (up_r \pm vp_s)\omega_r \\ & \times \left[\left(\frac{1}{vp_s+2} R_m^{vp_s+2} + R_r^{2vp_s} \frac{1}{-vp_s+2} R_m^{-vp_s+2} \right) \right. \\ & \left. - \left(\frac{1}{vp_s+2} R_r^{vp_s+2} + R_r^{2vp_s} \frac{1}{-vp_s+2} R_r^{-vp_s+2} \right) \right] \\ & \times \left\{ \cos\left[(up_r \pm vp_s)\omega_r t \pm vp_s \frac{\alpha_p}{2} + \theta_u \right] \right. \\ & \left. - \cos\left[(up_r \pm vp_s)\omega_r t \mp vp_s \frac{\alpha_p}{2} + \theta_u \right] \right\}. \end{aligned} \tag{7}$$

Table 1. Comparison of losses in a SPMSM.

Name	Analytical model	FEA
Eddy current loss in the magnets	93 W	102 W

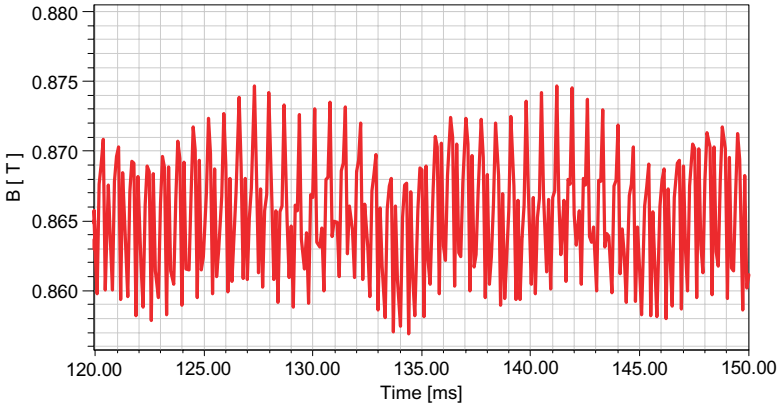

Fig. 2. Flux distribution in the magnet of SPMSM obtained from time stepped FEA. The flux density is measured at the center of the magnet.

Finally, the eddy current loss in one magnet per unit axial length can be obtained,

$$P = \frac{\omega_r}{2\pi} \int_0^{2\pi/\omega_r} \int_{R_r}^{R_m} \int_{-\alpha/2}^{\alpha/2} \frac{1}{\sigma} J_m^2 r dr d\theta_r dt \,. \tag{8}$$

To validate the analytical method, the eddy current loss of a SPMSM is also obtained from time-stepped finite element analysis (FEA) and compared with the results from the analytical model as shown in Table 1. The flux density in the magnets of the SPMSM is shown in Fig. 2. It can be seen that the results from the analytical model assembles the FEA results very well. Therefore, the analytical model is validated.

3. Eddy Current Loss in the Magnets of IPMSM

The Toyota Prius HEV traction motor shown in Fig. 3 uses interior magnets. It is essentially an IPMSM which has become more and more popular in vehicular traction motor drives.

For IPMSM, the eddy current loss calculation is rather complicated due to the fact that the magnets are buried inside the rotor body unlike SPMSM in which the magnets are mounted on the surface of the rotor. Hence the following equation is used to calculated the eddy current loss in the magnet of an IPMSM,[24]

$$P = \frac{2la}{\sigma\delta}|H|^2 \frac{b+l}{b} = \frac{2la}{\sigma\delta}|\mu H|^2 \frac{b+l}{b} = \frac{2la}{\sigma\delta\mu^2}|B|^2 \frac{b+l}{b} \,. \tag{9}$$

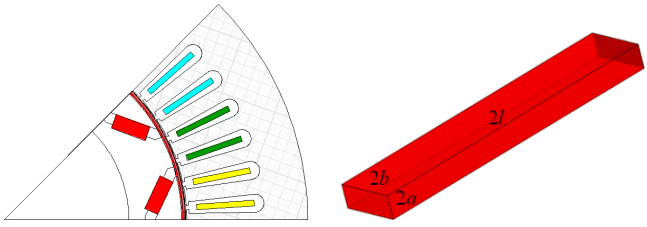

Fig. 3. Magnet structure of IPMSM.

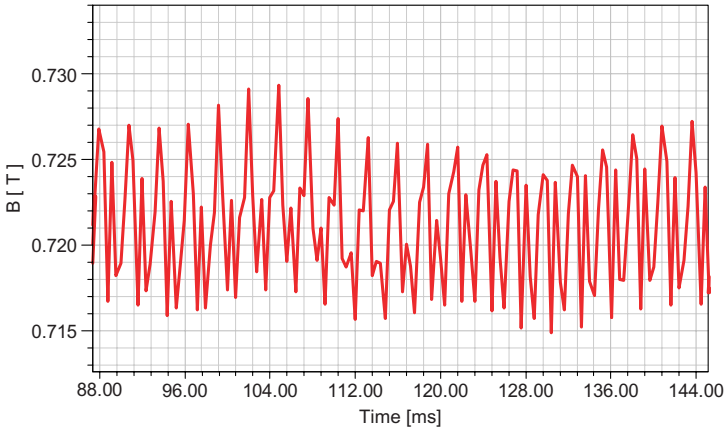

Fig. 4. The flux distribution in the magnet of IPMSM obtained from time stepped FEA. The flux density is measured at the center of the magnet.

where a, b and l are one half of the thickness, width and length of the conductor shown in Fig. 3. δ is the skin depth and much smaller than b and l. μ is the relative magnetic permeability and B is the uniform flux density.

The flux density in the center of the magnet of an IPMSM is obtained from time-stepped FEA and shown in Fig. 4. The waveform obtained from FEA is used to calculate the eddy current loss in the magnet of an IPMSM.

4. Loss Due to PWM Supply

PWM inverters are often used to operate electrical machines to achieve variable speed drives. A limitation though with such technologies is the abundant high frequency harmonics in the output voltage of a PWM inverter, which induce additional losses. The eddy current loss due to the PWM supply can be many times the loss under pure sine wave supply.[3] Therefore, an excessive temperature-rise of electrical machines can be observed due to PWM supplies. It is critical to predict the losses caused by PWM supply in various parts of the machine due to PWM harmonics.

The output voltage of a PWM waveform contains the fundamental voltage, carrier frequency-related harmonics and other high frequency harmonic voltages. The general Fourier series of the output voltage is given as Ref. 3,

$$v(t) = \sum_{n=1}^{\infty} v_n(t) = \sum_{n=1}^{\infty} (a_n \cos n\omega t + b_n \sin n\omega t) = \sum_{n=1}^{\infty} v_n \sin(n\omega t + \varphi_n)\,. \tag{10}$$

where ω is fundamental angular frequency, n is the order of harmonics, V_n is the amplitude of the nth harmonic, a_n and b_n are the Fourier coefficients and φ_n is the phase angle of the nth harmonic.

In order to delineate the analytical expression of the harmonic voltages, the output voltage of the PWM is separated from harmonic voltages and used to further calculate the eddy current losses caused by the PWM voltage harmonics. The calculated eddy current losses in the magnets of IPMSM are shown in Fig. 5.

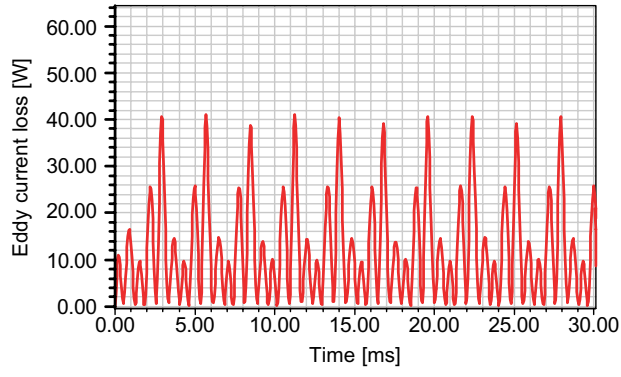

(a)

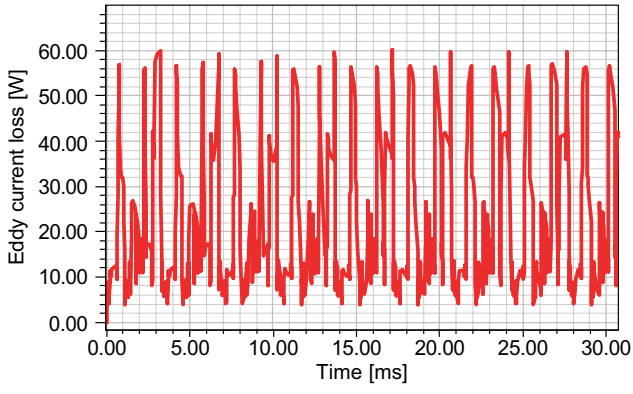

(b)

Fig. 5. Comparison of eddy current loss in IPMSM calculated by time-stepped FEA. (a) IPMSM fed by sine supply. (b) IPMSM fed by PWM supply.

5. Lumped-Parameter Thermal Model of SPMSM

The thermal lumped-parameter thermal model for SPMSM and IPMSM were developed as shown in Fig. 6. The thermal capacitances have been neglected since only the steady state operation of the machine is considered.

Variables T_{in}, T_{stator}, T_{magnet}, T_{rotor}, T_w, and T_{shaft} describe the temperatures of inner surface of insulation between stator and casing, inner surface of the stator core, outer surface of magnet, outer surface of rotor, the part of winding within the stator core and the part of shaft under rotor core respectively. T_{coolant} and T_{case} are assigned as boundary conditions. Furthermore, the use of the individual thermal resistance as illustrated in Table 2 facilitates the development of the distinct analytical expressions and detailed value which is included in Ref. 37. The thermal resistances of the poles and the rotor core are combined together in IPMSM, as shown in Table 2.

6. Validation of the Loss Model

Table 3 gives the basic parameters of the SPMSM and IPMSM. In order to compare the increment of losses under PWM supply, the fundamental frequency and amplitude of the PWM supply are kept the same as the pure sinusoidal waveform.

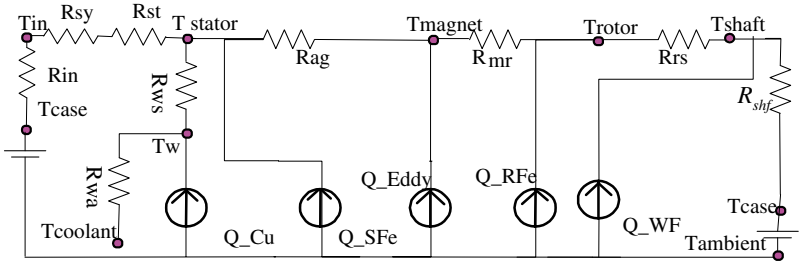

(a)

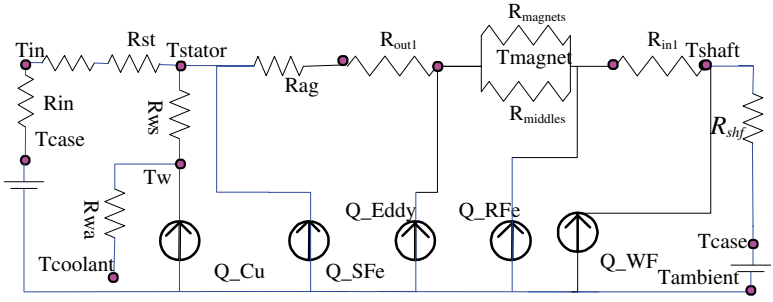

(b)

Fig. 6. Equivalent thermal circuit. (a) SPMSM; (b) IPMSM.

Table 2. Thermal resistances.

Name	Depiction	SPMSM (°C/W)	IPMSM (°C/W)
R_{ag}	Thermal resistance of air gap	0.0240	0.0019
R_{mr}	Radial conduction thermal resistance of the pole	0.0200	0.0122*
R_{rs}	Radial conduction thermal resistance of rotor core	0.0220	
R_{shf}	Thermal resistance of the shaft	0.4290	0.3560
R_{sy}	Radial conduction thermal resistance of stator yoke	0.0056	0.0049
R_{st}	Radial conduction thermal resistance of stator teeth	0.0160	0.0170
R_{ws}	Conduction thermal resistance between windings and stator	0.0200	0.0120
R_{in}	Thermal resistance of housing	0.0210	0.0180

*Combined thermal resistances of the poles and the rotor core.

Table 3. Basic parameters of the IPMSM and SPMSM.

Parameter	SPMSM	IPMSM
Peak power	50 kW	50 kW
Pole number	8	8
Speed	3600 rpm	900 rpm
Slot fill factor	0.74	0.84
Number of slots	48	48
Outer radius of stator	135.0 mm	134.95 mm
Inner radius of stator	81.1 mm	80.9 mm
Length of stator core	84.0 mm	83.8 mm
Switching frequency	3.6 kHz	0.9 kHz

The frequency modulation ratio is R, $R = f_c/f_1$, f_c is the frequency of the triangle waveform and f_1 is the frequency of the fundamental sinusoidal modulation waveform.

The amplitude modulation ratio is M, $M = V_1/V_c$, V_1 is the amplitude of the sinusoidal waveform and V_c is the amplitude of triangle waveform. R and M are set as 15 and 0.9, respectively.

The losses and efficiency of the IPMSM was calculated using the time stepped FEA as shown in Table 4, and compared with the results from Oak ridge national laboratory (ORNL) report.[28] In the ORNL experiment, the input to the motor was also a pure sinusoidal waveform supplied from an autotransformer which is connected directly to a 60 Hz three-phase line input. Except for the eddy current loss in magnets, all the losses are obtained from their experiments. The eddy current loss in magnets was assumed as a constant value in their research. It can be seen that, save for the loss in the magnets, the analytical results are consistent with the measurements. Since the ORNL report did not measure the loss in the magnets, it cannot therefore be used to validate the calculations in this paper.

The losses under sinusoidal waveform and under PWM supply are further calculated for both the IPMSM and the SPMSM using the analytical models developed and the time stepped FEA, as shown in Tables 5 and 6. Both Tables 5 and 6 show

Table 4. Comparison of losses from time stepped FEA and measurement under sine wave supply for the IPMSM.

Name	Measurement	Simulation
Eddy current loss in the magnets	40 W	10.5 W
Input power	17354.6 W	16469.7 W
Output power	15042 W	14202 W
Efficiency	0.87	0.86
Current	78 A	77.5 A
Torque	159.6 Nm	150.7 Nm
Stator iron loss	952 W	947 W
Copper loss	935 W	928.7 W
Rotor iron loss	225.6	221.5 W
Friction and windage loss	160 W	160 W

Table 5. Losses under sine and PWM waveform for IPMSM from calculation.

Name	Sine	PWM
Eddy current loss in the magnets†	9.8 W	20.5 W
Eddy current loss in the magnets‡	10.5 W	24.6 W
Input power	16469.7 W	17421.8 W
Output power	14202 W	14004 W
Efficiency	0.86	0.80
Current (fundamental)	77.5 A	77.1 A
Torque	150.7 Nm	148.6 Nm
Stator iron loss	947 W	1832.6 W
Copper loss	928.7 W	935.1 W
Rotor iron loss	221.5 W	465.5 W
Friction and windage loss	160 W	160 W

†Eddy current loss in the magnets was calculated by analytical method.
‡Eddy current loss in the magnets was calculated through time stepped FEA.

Table 6. Losses under sine and PWM waveform for SPMSM from calculation.

	Sine	PWM
Eddy current loss in the magnets§	0.093 kW	0.227 kW
Eddy current loss in the magnets¶	0.102 kW	0.249 kW
Input power	53.586 kW	53.706 kW
Output power	51.644 kW	50.136 kW
Efficiency	96.4%	93.4%
Stator iron loss	1.091 kW	2.723 kW
Stator copper loss	0.245 kW	0.253 kW
Rotor iron loss	0.188 kW	0.345 kW
Friction and windage loss	0.316 kW	0.316 kW

§Eddy current loss in magnets was calculated by analytical method.
¶Eddy current loss in magnets was calculated through time stepped FEA.

that the losses in the motors by PWM waveform are twofold in magnitude in relation to the losses under sinusoidal supply, with the exception being the copper loss, and friction and windage losses. These results are consistent with the previous work.[3]

The loss in the magnets in both SPMSM and IMPSM are doubled in the case of PWM supply, compared to pure sine wave supply, as confirmed by both analytical method and time stepped FEA. This indicates a necessity for developing design constraints of PM traction motors so that the magnets are not exposed to excessive temperature-rise, nor the motor performance degrade due to irreversible loss of magnetic property.

7. The Temperature-Rise within the Machines

Assigning the losses and casing temperature (90°C) to the thermal circuits, the temperature of individual components in the machines can be obtained.

Consider the equivalent circuit model in Fig. 6, At node T_{in}

$$\frac{T_{\text{stator}} - T_{\text{in}}}{R_{sy} + R_{st}} - \frac{T_{\text{in}} - T_{\text{case}}}{R_{\text{in}}} = 0\,. \tag{11}$$

At node T_{stator}

$$\frac{T_{\text{stator}} - T_{\text{in}}}{R_{sy} + R_{st}} - \frac{T_w - T_{\text{stator}}}{R_{ws}} \frac{T_{\text{magnet}} - T_{\text{stator}}}{R_{ag}} = Q\_SFe\,. \tag{12}$$

At node T_w

$$\frac{T_w - T_{\text{stator}}}{R_{ws}} - \frac{T_w - T_{\text{coolant}}}{R_{wa}} = Q\_Cu\,. \tag{13}$$

At node T_{magnet}

$$\frac{T_{\text{magnet}} - T_{\text{stator}}}{R_{ag}} - \frac{T_{\text{rotor}} - T_{\text{magnet}}}{R_{mr}} = Q\_Eddy\,. \tag{14}$$

At node T_{rotor}

$$\frac{T_{\text{rotor}} - T_{\text{shaft}}}{R_{rs}} + \frac{T_{\text{rotor}} - T_{\text{magnet}}}{R_{mr}} = Q\_RFe + Q\_WF\,. \tag{15}$$

At node T_{shaft}

$$\frac{T_{\text{rotor}} - T_{\text{shaft}}}{R_{rs}} - \frac{T_{\text{shaft}} - T_{\text{case}}}{R_{shf}} = 0\,. \tag{16}$$

The system equations (11)−(16) can be used to calculate the node temperatures for the SPMSM. The analogous system equations can also be developed for the IPMSM. From Ref. 37, $k_{cu,ir}$ is the equivalent conductivity coefficient of the air and the insulation material in stator slot and could not be computed directly. A program for

Table 7. Comparison of temperature distribution from analytical model and measurements under sinusoidal supply for the IPMSM.

	Measurement (°C)	Analytical model (°C)
Stator core	133.73∼157	127.8∼149.5
Winding	160.81∼167.6	143.8
Rotor core	154.4∼157.6	146.6∼149.3
Magnets	157.2∼158.1	149.3∼150.7

Table 8. Temperature distribution under sine and PWM within SPMSM from calculation.

	Sine (°C)	PWM (°C)
Insulation	90∼113.23	90∼159.14
Stator	113.23∼152.35	159.14∼198.25
Winding	155.29	202.47
Magnets	154.88∼155.47	200.92∼201.54
Rotor	155.47∼169.76	201.54∼213.83
Shaft	90∼169.76	90∼213.83

Table 9. Temperature distribution under sine and PWM for the IPMSM from calculation.

	Sine (°C)	PWM (°C)
Stator core	127.8∼149.5	168.6∼189.2
Winding	143.8	195.6
Rotor core	146.6∼149.3	185.9∼192.3
Magnets	149.3∼150.7	192.3∼193.9

solving the system equations matrix is developed, and the value of $k_{cu,ir}$ is changed until the computed temperatures is comparable with the report from ORNL.

Table 7 shows the comparison of the temperature-rise of the IPMSM calculated using the developed analytical model, and the results from the experiment conducted by ORNL. The results are consistent which validates the analytical model.

The temperature distribution within the SPMSM and IPMSM are further calculated for sinusoidal and PWM supplies, as shown in Tables 8 and 9. The temperature is dramatically higher under PWM with the same boundary condition used in the thermal circuits. This is due to the excessive losses caused by PWM supply in the machines. The hottest portion of magnets ascends to around 200°C, which may induce irreversible demagnetization. These results provide the crucial information for the motor design. Minimization of the losses within the motor[29−36] and improvement of the coolant system can be used to restrain the temperature-rise.

8. Conclusion

With sinusoidal and PWM supplies, analytical models of eddy current losses in magnets are presented for SPMSM and IPMSM respectively. Based on the eddy

current losses combined with other losses within the machines, the thermal models are developed to predict the temperature-rise in individual components of the SPMSM and IPMSM, respectively. The eddy current loss predicted by the two analytical models is validated by the results from time-stepped FEA. Furthermore, the analytical eddy current loss model and the thermal model of the IPMSM are validated by the results from the ORNL report, providing a reliable method to predict the temperature-rise.

References

1. S. M. Jang, U. H. Lee, D. J. You, J. P. Lee and S. H. Choi, Operating torque estimation of high-speed slotless brushless DC machine considering power loss, *IEEE Trans. Magnetics* **45** (2009) 4539−4542.
2. K. Yamazaki and Y. Kanou, Rotor loss analysis of interior permanent magnet motors using combination of 2-D and 3-D finite element method, *IEEE Trans. Magnetics* **45** (2009) 1772−1775.
3. R. F. Liu, C. Mi and D. W. Gao, Modeling of eddy-current loss of electrical machines and transformers operated by pulsewidth-modulated inverters, *IEEE Trans. Magnetics* **44** (2008) 2021−2028.
4. K. Yoshida, Y. Hita and K. Kesamaru, Eddy-current loss analysis in PM of surface-mounted-PM SM for electric vehicles, *IEEE Trans. Magnetics* **36** (2000) 1941−1944.
5. D. Ishak, Z. Q. Zhu and D. Howe, Eddy-current loss in the rotor magnets of permanent-magnet brushless machines having a fractional number of slots per pole, *IEEE Trans. Magnetics* **41** (2005) 3728−3726.
6. M. Haavisto and M. Paju, Temperature stability and flux losses over time in sintered Nd−Fe−B permanent magnets, *IEEE Trans. Magnetics* **45** (2009) 5277−5280.
7. J. Wang, W. Wang, K. Atallah and D. Howe, Demagnetization assessment for three-phase tubular brushless permanent-magnet machines, *IEEE Trans. Magnetics* **44** (2008) 2195−2203.
8. J. Faiz, B. Ganji, C. E. Carstensen, K. A. Kasper and R. W. De Doncker, Temperature rise analysis of switched reluctance motors due to electromagnetic losses, *IEEE Trans. Magnetics* **45** (2009) 2927−2934.
9. Y. K. Huang, J. G. Zhu and Y. G. Guo, Thermal analysis of high-speed SMC motor based on thermal network and 3-D FEA with rotational core loss included, *IEEE Trans. Magnetics* **45** (2009) 4680−4683.
10. A. Boglietti, A. Cavagnino, M. Lazzari and M. Pastorelli, A simplified thermal model for variable speed self cooled industrial induction motor, *37th IAS Annual Meeting. Conference, Record of the Industry Applications Conf.*, Vol. 2 (2002), pp. 723−730.
11. S. C. Tang, T. A. Keim and D. J. Perreault, Thermal modeling of Lundell alternators, *IEEE Trans. Energy Conversion* **20** (2005) 25−36.
12. G. Sooriyakumar, R. Perryman and S. J. Dodds, Analytical thermal modelling for permanent magnet synchronous motors, *42nd Int. Universities Power Engineering Conf.* (2007), pp. 192−196.
13. D. Staton, A. Boglietti and A. Cavagnino, Solving the more difficult aspects of electric motor thermal analysis in small and medium size industrial induction motors, *IEEE Trans. Energy Conversion* **20** (2005) 620−628.

14. B. Funieru and A. Binder, Thermal design of a permanent magnet motor used for gearless railway traction, *34th Annual Conf. IEEE Industrial Electronics* (2008), pp. 2061−2066.
15. D. A. Staton and A. Cavagnino, Convection heat transfer and flow calculations suitable for electric machines thermal models, *IEEE Trans. Industrial Electron.* **55** (2008) 3509−3516.
16. A. Cassat, C. Espanet and N. Wavre, BLDC motor stator and rotor iron losses and thermal behavior based on lumped schemes and 3-D FEM analysis, *IEEE Trans. Ind. Appl.* **39** (2003) 1314−1322.
17. W. G. Kim, J. I. Lee, K. W. Kim, Y. S. Kim and C. D. Lee, The temperature-rise characteristic analysis technique of the traction motor for EV application, *The 1st Int. Forum on Strategic Technology*, Vols. 18−20 (2006), pp. 443−446.
18. S. K. Chowdhury, A distributed parameter thermal model for induction motors, *Int. Conf. Power Electronics and Drives Systems*, Vol. 1 (2005), pp. 739−744.
19. K. Atallah, D. Howe, P. H. Mellor and D. A. Stone, Rotor loss in permanent magnet brushless AC machines, *IEEE Trans. Ind. Appl.* **36** (2000) 1612−1618.
20. Z. Q. Zhu, K. Ng, N. Schofield and D. Howe, Improved analytical modelling of rotor eddy current loss in brushless machines equipped with surface mounted permanent magnets, *IEEE Proc.-Electr. Power Appl.* **151** (2004) 641−650.
21. H. Toda, Z. P. Xia, J. B. Wang, K. Atallah and D. Howe, Rotor eddy-current loss in permanent magnet brushless machines, *IEEE Trans. Magnetics* **40** (2004) 2104−2106.
22. Z. Q. Zhu, D. Howe, E. Bolte and B. Ackermann, Instantaneous magnetic field distribution in brushless permanent magnet dc motors, Part I: Open-circuit field, *IEEE Trans. Magnetics* **29** (1993) 124−135.
23. Z. Q. Zhu and D. Howe, Instantaneous magnetic field distribution in brushless permanent magnet dc motors, Part II Armature-reaction field, *IEEE Trans. Magnetics* **29** (1993) 136−143.
24. K. Yamazaki and A. Abe, Loss analysis of interior permanent magnet motors considering carrier harmonics and magnet eddy currents using 3-D FEM, *Electric Machines & Drives Conf.*, Vol. 2 (2007), pp. 904−909.
25. G. I. Taylor, Distribution of velocity and temperature between concentric cylinders, *Proc. Roy. Soc.* 1935, 159, Pt. A, pp. 546−578.
26. Gazley, Heat transfer characteristics of rotational and axial flow between concentric cylinder, *Trans. ASME* (1958), pp. 79−89.
27. P. H. Mellor, D. Roberts and D. R. Turner, Lumped parameter thermal model for electrical machines of TEFC design, *IEEE Proc.-B Electr. Power Appl.* **138** (1991) 205−218.
28. J. S. Hsu, S. C. Nelson, P. A. Jallouk, C. W. Ayers, R. H. Wiles, S. L. Campbell, C. L. Coomer, K. T. Lowe and T. A. Burress, Report on Toyota Prius Motor Thermal Management (2005), http://www.ornl.gov/∼webworks/cppr/y2001/rpt/122586.pdf.
29. C. Mi, G. R. Slemon and R. Bonert, Minimization of iron losses of permanent magnet synchronous machines, *IEEE Trans. Energy Conversion* **20** (2005) 121−127.
30. G. W. Zhang, F. X. Wang and Y. S. Shen, Reduction of rotor loss and cogging torque of high speed PM machine by stator teeth notching, *Int. Conf. Electrical Machines and Systems*, Vols. 8−11 (2007), pp. 856−859.
31. J. D. Park, C. Kalev and H. F. Hofmann, Analysis and reduction of time harmonic rotor loss in solid-rotor synchronous reluctance drive, *IEEE Trans. Power Electron.* **23** (2008) 985−992.

32. K. Yamazaki and H. Ishigami, Reduction of harmonic iron losses in interior permanent magnet motors by optimization of rotor structures, *ICEMS 2008. Int. Conf. Electrical Machines and Systems*, Vols. 17−20 (2008), pp. 2870−2875.
33. K. Yamazaki, M. Shina, Y. Kanou, M. Miwa and J. Hagiwara, Effect of eddy current loss reduction by segmentation of magnets in synchronous motors: Difference between interior and surface types, *IEEE Trans. Magnetics* **45** (2009) 4756−4759.
34. P. Sergeant and A. Van den Bossche, Segmentation of magnets to reduce losses in permanent-magnet synchronous machines, *IEEE Trans. Magnetics* **44** (2008) 4409−4412.
35. K. Yamazaki, M. Shina, M. Miwa and J. Hagiwara, Investigation of eddy current loss in divided Nd−Fe−B sintered magnets for synchronous motors due to insulation resistance and frequency, *IEEE Trans. Magnetics* **44** (2008) 4269−4272.
36. N. Takahashi, H. Shinagawa, D. Miyagi, Y. Doi and K. Miyata, Analysis of eddy current losses of segmented Nd−Fe−B sintered magnets considering contact resistance, *IEEE Trans. Magnetics* **45** (2009) 1234−1237.
37. X. F. Ding, M. Bhattacharya 1 and C. T. Mi, Simplified thermal model of pm motors in hybrid vehicle applications taking into account eddy current loss in magnets, *J. Asia Electr. Vehic.* **8** (2010) 1−7.